



Measurement of the ratio of B_c^+ branching fractions to $J/\psi\pi^+$ and $J/\psi\mu^+\nu_\mu$ final states

The LHCb collaboration[†]

Abstract

The first measurement that relates semileptonic and hadronic decay rates of the B_c^+ meson is performed using proton-proton collision data corresponding to 1.0 fb^{-1} of integrated luminosity collected with the LHCb detector. The measured value of the ratio of branching fractions, $\mathcal{B}(B_c^+ \rightarrow J/\psi\pi^+)/\mathcal{B}(B_c^+ \rightarrow J/\psi\mu^+\nu_\mu) = 0.0469 \pm 0.0028 \text{ (stat)} \pm 0.0046 \text{ (syst)}$, is at the lower end of available theoretical predictions.

Submitted to Physical Review D

© CERN on behalf of the LHCb collaboration, license CC-BY-4.0.

[†]Authors are listed at the end of this paper.

1 Introduction

The B_c^+ meson is the ground state of the $\bar{b}c$ quark-pair system and is the only meson in which weak-interaction decays of both constituents compete with each other.¹ About 70% of the decay width is expected to be due to the $c \rightarrow s$ transition, favored by the Cabibbo-Kobayashi-Maskawa quark-coupling hierarchy [1]. This decay process has recently been observed in the $B_c^+ \rightarrow B_s^0 \pi^+$ mode [2]. The complementary $b \rightarrow c$ transition, which is predicted to account for 20% of the decay width, is more straightforward to observe experimentally, having a substantial probability to produce a J/ψ meson. Among such decays, semileptonic $B_c^+ \rightarrow J/\psi \ell^+ \nu_\ell$ ($\ell = \mu, e$) and hadronic $B_c^+ \rightarrow J/\psi \pi^+$ channels have played a special role in many measurements. The semileptonic decays were used in the discovery of the B_c^+ meson [3], the measurements of its lifetime [3–6] and the measurement of the production cross-section at the Tevatron [3]. The $B_c^+ \rightarrow J/\psi \pi^+$ decays were used to measure its lifetime [7], mass [8–10], production cross-section at the LHC [10] and as a reference for other hadronic branching fraction measurements [11–16]. However, there is no experimental determination of the relative size of semileptonic and hadronic decay rates. The goal of this work is a measurement of the ratio of branching fractions,

$$\mathcal{R} \equiv \frac{\mathcal{B}(B_c^+ \rightarrow J/\psi \pi^+)}{\mathcal{B}(B_c^+ \rightarrow J/\psi \mu^+ \nu_\mu)}, \quad (1)$$

and to test various theoretical models of B_c^+ meson decays, for which predictions of \mathcal{R} vary over a wide range, 0.050–0.091 [17–24].

2 Analysis outline

Final states containing a muon offer a distinctive experimental signature and can be triggered and reconstructed with high efficiency at LHCb. Therefore, this analysis relies on J/ψ decays to $\mu^+ \mu^-$. Since the neutrino is not detected, both of the studied decay modes are reconstructed using a J/ψ candidate plus a charged track (t^+), referred to as the *bachelor* track. The mass of $J/\psi \pi^+$ signal candidates peaks at the B_c^+ mass within the experimental resolution, allowing a straightforward signal yield extraction in the presence of relatively small backgrounds under the signal peak. The main challenge in this analysis is the signal yield extraction for the $B_c^+ \rightarrow J/\psi \mu^+ \nu_\mu$ decay mode, as the $J/\psi \mu^+$ mass ($m_{J/\psi \mu}$) distribution is broad due to the undetected neutrino. To suppress the dominant backgrounds, the analysis is restricted to the $m_{J/\psi \mu} > 5.3$ GeV endpoint region and uses the mass-shape difference between the signal and the remaining background to extract the $B_c^+ \rightarrow J/\psi \mu^+ \nu_\mu$ signal yield.² In this mass region the neutrino has low energy, thus the $B_c^+ \rightarrow J/\psi \mu^+ \nu_\mu$ candidates are kinematically similar to the $B_c^+ \rightarrow J/\psi \pi^+$ candidates. Therefore, many reconstruction uncertainties cancel in the ratio of their rates, allowing a precise measurement of $\mathcal{R}(m_{J/\psi \mu} > 5.3$ GeV). This endpoint value is then extrapolated to

¹Charge-conjugate states are implied in this article.

²Units in which $c = 1$ are used.

the full phase space using theoretical predictions. Since the B_c^+ and J/ψ are both $1S$ heavy quarkonia states, the form factors involved in predicting the extrapolation factor and the shape of the mass distribution at the endpoint have only modest model dependence.

3 Detector and data sample

The analysis is performed on a data sample of pp collisions at a center-of-mass energy of 7 TeV, collected during 2011 by the LHCb experiment and corresponding to an integrated luminosity of 1.0fb^{-1} . The LHCb detector [25] is a single-arm forward spectrometer covering the pseudorapidity range $2 < \eta < 5$, designed for the study of particles containing b or c quarks. The detector includes a high-precision tracking system consisting of a silicon-strip vertex detector surrounding the pp interaction region [26], a large-area silicon-strip detector located upstream of a dipole magnet with a bending power of about 4 Tm, and three stations of silicon-strip detectors and straw drift tubes [27] placed downstream of the magnet. The tracking system provides a measurement of momentum, p , with a relative uncertainty that varies from 0.4% at low momentum to 0.6% at 100 GeV. The minimum distance of a track to a primary vertex, the impact parameter (IP), is measured with a resolution of $(15 + 29/p_T)\mu\text{m}$, where p_T is the component of p transverse to the beam, in GeV. Different types of charged hadrons are distinguished using information from two ring-imaging Cherenkov detectors [28]. Photon, electron and hadron candidates are identified by a calorimeter system consisting of scintillating-pad and preshower detectors, an electromagnetic calorimeter and a hadronic calorimeter. Muons are identified by a system composed of alternating layers of iron and multiwire proportional chambers [29].

Simulated event samples are generated for the signal decays and the decay modes contributing to the background. In the simulation, pp collisions are generated using PYTHIA [30] with a specific LHCb configuration [31]. The production of B_c^+ mesons, which is not adequately simulated in PYTHIA, is performed by the dedicated generator BCVEGPY [32]. Several dynamical models are used to simulate $B_c^+ \rightarrow J/\psi \mu^+ \nu_\mu$ decays. Decays of hadronic particles are described by EVTGEN [33], in which final-state radiation is generated using PHOTOS [34]. The interaction of the generated particles with the detector and its response are implemented using the GEANT4 toolkit [35] as described in Ref. [36].

4 Data selection

This analysis relies on $J/\psi t^+$ candidates satisfying the trigger [37], which consists of a hardware stage, based on information from the muon system, followed by a two-level software stage, which applies a full event reconstruction. At the hardware stage, a muon with $p_T > 1.5\text{ GeV}$, or a pair of muons with $\sqrt{p_{T1}p_{T2}} > 1.3\text{ GeV}$, is required. The subsequent lower-level software triggers require a charged-particle track with $p_T > 1.7\text{ GeV}$ ($p_T > 1.0\text{ GeV}$ if identified as muon) and with an IP relative to any primary pp -interaction vertex (PV) larger than $100\ \mu\text{m}$. A dimuon trigger, which requires a large dimuon mass,

$m_{\mu^+\mu^-} > 2.7$ GeV, and each muon to have $p_T > 0.5$ GeV, complements the single track triggers. The final software trigger stage requires either a $J/\psi \rightarrow \mu^+\mu^-$ candidate with a J/ψ decay vertex separation from the nearest PV of at least three standard deviations, or that a two- or three-track combination, which includes a muon, is identified as a secondary vertex using a multivariate selection [37].

In the offline analysis, $J/\psi \rightarrow \mu^+\mu^-$ candidates are selected with the following criteria: $p_T(\mu) > 0.9$ GeV; $p_T(J/\psi) > 1.5$ GeV; χ^2 per degree of freedom (ndf) for the two muons to form a common vertex $\chi_{\text{vtx}}^2(\mu^+\mu^-)/\text{ndf} < 9$; and a mass consistent with the J/ψ meson. The separation of the J/ψ decay vertex from the nearest PV must be at least five standard deviations. The bachelor track, and at least one of the muons from the decay of the J/ψ meson, must not point to any PV, through the requirement $\chi_{\text{IP}}^2 > 9$. The quantity χ_{IP}^2 is defined as the difference between the χ^2 of the PV fitted with and without the considered particle. The bachelor track must not be collinear within 0.8° with either of the muons from the J/ψ meson decay and must satisfy $p_T > 0.5$ GeV (> 1.0 GeV for π^+). A loose kaon veto is applied to the pion candidates, $\ln[\mathcal{L}(K)/\mathcal{L}(\pi)] < 5$, where \mathcal{L} is the particle identification likelihood [38]. The J/ψ candidates are combined with the bachelor tracks in a kinematic fit to form B_c^+ candidates with the known J/ψ mass and the B_c^+ vertex used as constraints. The B_c^+ candidate must satisfy $\chi_{\text{vtx}}^2(J/\psi t^+)/\text{ndf} < 9$ and have a pseudo-proper decay time greater than 0.25 ps. The pseudo-proper decay time is determined as $L \cdot m_{J/\psi t} / |\vec{p}_{J/\psi t}|$, where L is the projection of the distance between the B_c^+ production and decay vertices onto the direction of the $J/\psi t^+$ momentum $\vec{p}_{J/\psi t}$ and $m_{J/\psi t}$ is the $J/\psi t^+$ mass.

Four discriminating variables (x_i) are used in a likelihood ratio to improve the background suppression. Three of the variables are common between the two channels: $\chi_{\text{vtx}}^2(J/\psi t^+)/\text{ndf}$, $\chi_{\text{IP}}^2(B_c^+)$, and the cosine of the angle between the J/ψ meson and the bachelor track transverse momenta. The latter quantity peaks at positive values for the signal as the B_c^+ meson has a high transverse momentum. Background events in which particles are combined from two different B decays usually peak at negative values, whilst those due to random combinations of particles are more uniformly distributed. The $\chi_{\text{IP}}^2(B_c^+)$ variable is small for $B_c^+ \rightarrow J/\psi \pi^+$ decays since the B_c^+ momentum points back to the PV. For $B_c^+ \rightarrow J/\psi \mu^+ \nu_\mu$ candidates, the pointing is only approximate since the neutrino is not reconstructed. However, $\chi_{\text{IP}}^2(B_c^+)$ is often smaller than for the background events because the neutrino has low momentum. The fourth variable for the $J/\psi \pi^+$ mode is $\chi_{\text{IP}}^2(t^+)$, while for the $J/\psi \mu^+ \nu_\mu$ mode it is the pseudo-proper decay time, as $\chi_{\text{IP}}^2(t^+)$ is found to be ineffective for this channel. The four one-dimensional signal probability density functions (PDFs), $\mathcal{P}_{\text{sig}}(x_i)$, are obtained from a simulated sample of signal events. The background PDFs, $\mathcal{P}_{\text{bkg}}(x_i)$, are obtained from the data in the $B_c^+ \rightarrow J/\psi \pi^+$ mass sidebands (5.35–5.80 and 6.80–8.50 GeV) and from the simulation of inclusive backgrounds from $B_{u,d,s} \rightarrow J/\psi X$ decays (X denotes one or more particles) for the $B_c^+ \rightarrow J/\psi \mu^+ \nu_\mu$ candidates. The requirement $\Delta_{\text{sig/bkg}}(-2\ln\mathcal{L}) = -2 \sum_{i=1}^4 \ln[\mathcal{P}_{\text{sig}}(x_i)/\mathcal{P}_{\text{bkg}}(x_i)] < 1.0$ (< 0.0) preserves about 93% (87%) of signal events for $B_c^+ \rightarrow J/\psi \pi^+$ ($B_c^+ \rightarrow J/\psi \mu^+ \nu_\mu$ with $m_{J/\psi \mu} > 5.3$ GeV) and efficiently suppresses the backgrounds. These requirements minimize the expected average statistical uncertainty on the signal yields, given the observed background levels in each

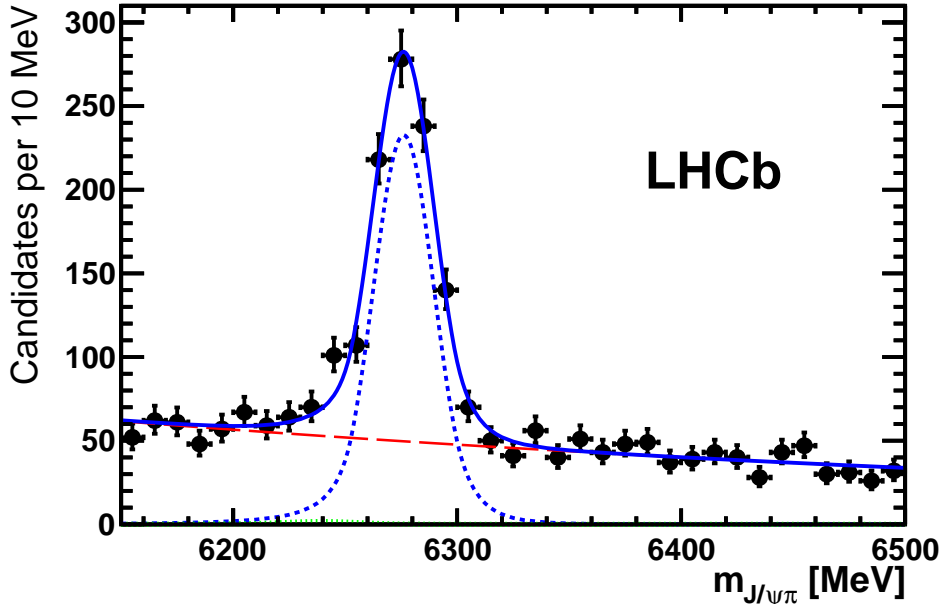


Figure 1: Invariant-mass distribution of $B_c^+ \rightarrow J/\psi \pi^+$ candidates (black data points). The maximum likelihood fit of the B_c^+ signal is superimposed (blue solid line). Individual fit components are also shown: (dashed blue line) the signal, (red long-dashed line) the background and (green dotted line) $B_c^+ \rightarrow J/\psi K^+$ feeddown.

channel.

5 Extraction of the $B_c^+ \rightarrow J/\psi \pi^+$ signal

An extended maximum likelihood fit to the unbinned distribution of observed $m_{J/\psi \pi}$ values yields $N_{J/\psi \pi} = 839 \pm 40$ $B_c^+ \rightarrow J/\psi \pi^+$ signal events and is shown in Fig. 1.

The signal is represented in the fit by a double-sided Crystal Ball (CB) function [39]. The peak position, the Gaussian mass resolution and the peak amplitude are free parameters in the fit, while the parameters describing small non-Gaussian tails are fixed by a fit to the simulated signal distribution. Using a Gaussian function to model the signal results in a 2.3% relative change in \mathcal{R} value, and this is assigned as the systematic uncertainty. The background is smoothly distributed and modeled by an exponential function. Varying the background parameterization and the fit range results in up to a 0.6% relative change in \mathcal{R} . A small background from $B_c^+ \rightarrow J/\psi K^+$ decays, peaking 37 MeV below the signal peak, is also included in the fit with all shape parameters fixed from the simulation. Its normalization is constrained to be 1% of the fitted signal amplitude, as predicted by the measured ratio of the branching fractions [14] scaled by an efficiency ratio of 15% obtained from the simulation. The relative systematic uncertainty on \mathcal{R} related to this fit component is 0.1%.

6 Extraction of the $B_c^+ \rightarrow J/\psi \mu^+ \nu_\mu$ signal

To measure the $B_c^+ \rightarrow J/\psi \mu^+ \nu_\mu$ rate, feeddown from other $B_c^+ \rightarrow f$, $f \rightarrow J/\psi \mu^+ \nu_\mu X$ decays must be accounted for. Decays to excited charmonium states ($f = \psi_f \mu^+ \nu_\mu$, with $\psi_f = \chi_{cJ}$ or $\psi(2S)$) and states containing τ leptons ($f = J/\psi \tau^+ \nu_\tau$) are the dominant contributions. Since the rates for such decays have not been measured, we rely on theoretical predictions for

$$R_f \equiv \frac{\mathcal{B}(B_c^+ \rightarrow f)}{\mathcal{B}(B_c^+ \rightarrow J/\psi \mu^+ \nu_\mu)}. \quad (2)$$

Although the spread in R_f predictions is large, the related systematic uncertainty is minimized by restricting the analysis to the high $J/\psi \mu^+$ mass region. Unreconstructed decay products in the $\psi_f \rightarrow J/\psi X$ transitions ($X = \gamma, \pi\pi, \pi^0, \eta, \gamma\gamma$) or $\tau^+ \rightarrow \mu^+ \nu_\mu \bar{\nu}_\tau$ decays carry energy away, lowering the $J/\psi \mu^+$ mass relative to that from direct $B_c^+ \rightarrow J/\psi \mu^+ \nu_\mu$ decays, as illustrated in Fig. 2. The selection requirement in $m_{J/\psi \mu}$ is chosen to eliminate the backgrounds from $B_{u,d,s}$ decays to J/ψ mesons associated with hadrons, with one of the hadrons misidentified as a muon. These backgrounds are large because the $B_{u,d,s}$ production rates are orders of magnitude higher than for B_c^+ . Since many exclusive decay modes with various hadron multiplicities and unknown branching ratios contribute, the $m_{J/\psi \mu}$ shape of such backgrounds is difficult to predict. The 5.3 GeV lower limit on $m_{J/\psi \mu}$ is above the kinematic limit for $B_u^+ \rightarrow J/\psi h^+$ decays, with h^+ denoting a charged kaon or pion, as illustrated in Fig. 2. The $B_{u,d,s}$ backgrounds in the selected region are much smaller, and are from $B_{u,d,s} \rightarrow J/\psi X$ decays paired with a bachelor μ^+ originating from a semileptonic decay of the companion b quark in the produced $b\bar{b}$ pair. Simulation of b -baryon decays to final states involving a J/ψ meson shows that they also contribute via this mechanism. The shape of such combinatorial backgrounds is less sensitive to the details of the composition of b -hadron decay modes, and thus is easier to predict. Since the combinatorial backgrounds are dominated by genuine muons, the analysis is not sensitive to the estimation of muon misidentification rates and associated systematic uncertainties.

The $m_{J/\psi \mu}$ signal shape is dominated by the endpoint kinematics, whereas the combinatorial background is smooth and extends beyond the kinematic limit for the $B_c^+ \rightarrow J/\psi \mu^+ \nu_\mu$ decays. The signal yield is determined by a fit to the $m_{J/\psi \mu}$ distribution. The feeddown background is small as discussed in detail below. Its shape is constrained by simulation, while its normalization is related to the signal yield via theoretical predictions. The unbinned maximum likelihood fit is performed simultaneously to the $m_{J/\psi \mu}$ distribution in data and the signal and background distributions from simulation, in the range of 5.3 to 8.0 GeV, and gives $N_{J/\psi \mu} = 3537 \pm 125$ signal events. The $m_{J/\psi \mu}$ distributions and the fit results are displayed in Fig. 3. The fit is described in detail below.

The total PDF used in the fit is the sum of the signal PDF (\mathcal{P}_{sig}), the feeddown background PDF (\mathcal{P}_{fd}) and the combinatorial background PDF (\mathcal{P}_{bkg}),

$$\mathcal{P}(m_{J/\psi \mu}) \propto N_{J/\psi \mu} (\mathcal{P}_{\text{sig}}(m_{J/\psi \mu}) + \alpha \mathcal{P}_{\text{fd}}(m_{J/\psi \mu})) + N_{\text{bkg}} \mathcal{P}_{\text{bkg}}(m_{J/\psi \mu}), \quad (3)$$

where α is the feeddown-to-signal yield ratio and N_{bkg} is the combinatorial background

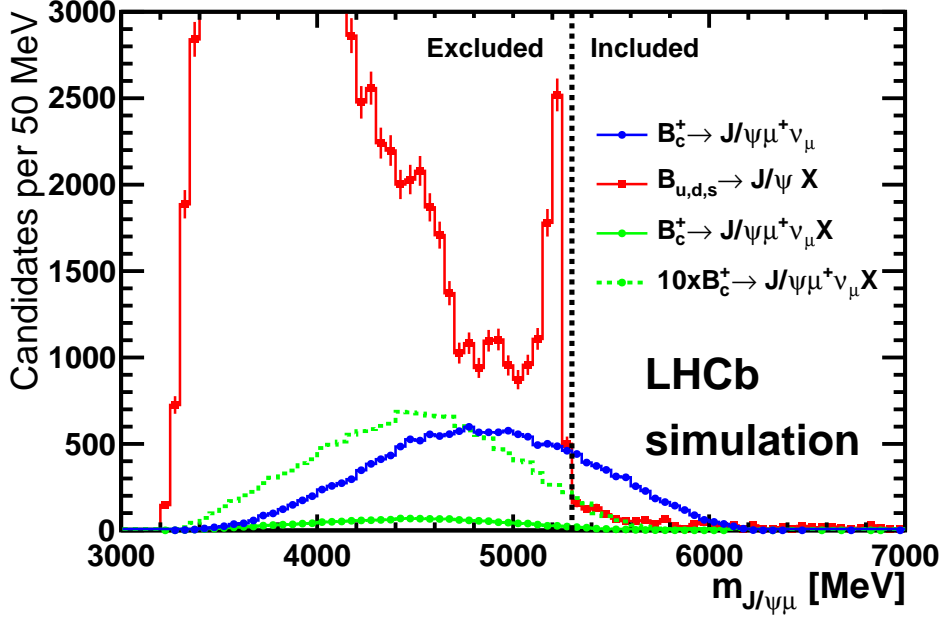


Figure 2: Distribution of $m_{J/\psi\mu}$ for $B_c^+ \rightarrow J/\psi\mu^+\nu_\mu$ candidates selected in simulated event samples of (blue filled points) the signal, (green filled points) the B_c^+ feddown and (red filled squares) the $B_{u,d,s}$ backgrounds. Relative normalization is derived from the fit to the data described later in the text. The part of the spectrum included in the fit is indicated with a vertical dashed black line. The B_c^+ feddown distribution is also shown after magnifying its normalization by a factor of ten (green dashed histogram).

yield. The signal shape is dominated by the endpoint kinematics, thus it is modeled as

$$\mathcal{P}_{\text{sig}}(m_{J/\psi\mu}) \propto \text{PS}(m_{J/\psi\mu}) (1 + s_1 \bar{m}_{J/\psi\mu}), \quad (4)$$

where $\bar{m}_{J/\psi\mu} = m_{J/\psi\mu} - 5.3 \text{ GeV}$ and $\text{PS}(m_{J/\psi\mu})$ corresponds to the uniform distribution in the $B_c^+ \rightarrow J/\psi\mu^+\nu_\mu$ three-body phase-space,

$$\text{PS}(m_{J/\psi\mu}) = \frac{M_{B_c}^2 - m_{J/\psi\mu}^2}{m_{J/\psi\mu}} \sqrt{m_{J/\psi\mu}^2 - (M_{J/\psi} + M_\mu)^2} \sqrt{m_{J/\psi\mu}^2 - (M_{J/\psi} - M_\mu)^2} \quad (5)$$

with the J/ψ and μ masses ($M_{J/\psi}$ and M_μ) set to their known values [40], and M_{B_c} set to an effective value, which is slightly higher than the B_c^+ mass to account for detector resolution effects. Setting M_{B_c} to the known B_c^+ mass [40] changes the signal yield by a negligible amount. Deviations from the uniform distribution are allowed by the linear term, with the s_1 coefficient determined by the simultaneous fit to the simulated signal distribution and the data. The simulation based on the Kiselev *et al.* QCD sum rules model [21] is used in the default fit. The models of Ebert *et al.* [22], based on a relativistic quasipotential Schrödinger approach, and ISGW2 [41], based on a nonrelativistic constituent quark model with relativistic corrections, alter the determined signal yield by +0.2% and -0.4%,

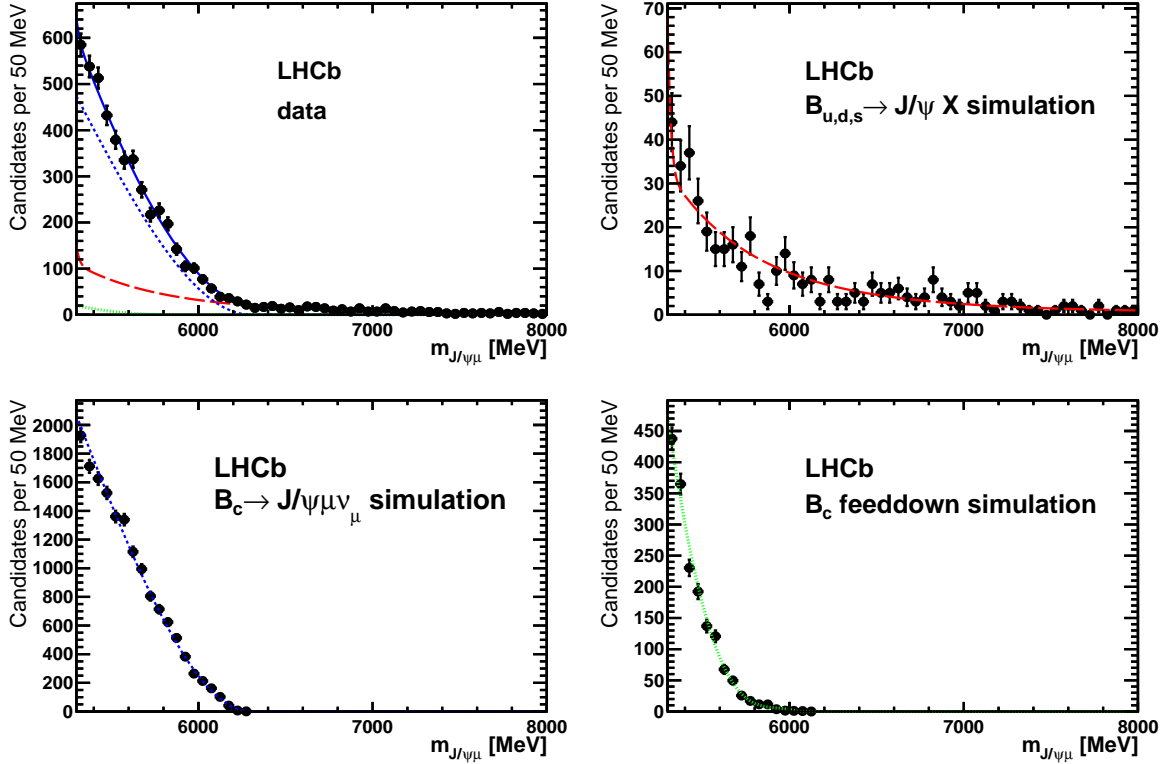


Figure 3: Invariant-mass distribution of $J/\psi\mu^+$ pairs from $B_c^+ \rightarrow J/\psi\mu^+\nu_\mu$ candidates (black data points) for (top left) the data, (bottom left) $B_c^+ \rightarrow J/\psi\mu^+\nu_\mu$ signal simulation, (top right) $B_{u,d,s} \rightarrow J/\psi X$ background simulation and (bottom right) B_c^+ feeddown simulation. The unbinned maximum likelihood fit of the B_c^+ signal is superimposed (blue solid line). Individual fit components are also shown: (blue short-dashed line) the signal, (red long-dashed line) the background and (green dotted line) B_c^+ feeddown.

respectively. Relying on the data themselves to determine the signal shape changes the signal yield by $+0.7\%$. The latter value is taken as a systematic error.

The feeddown includes contributions from the following B_c^+ decay modes $f = \psi(2S)\mu^+\nu_\mu$, $\chi_{cJ}\mu^+\nu_\mu$ and $J/\psi\tau^+\nu_\tau$. Feeddown from $B_c^+ \rightarrow B_{d,s}\mu^+\nu_\mu$ and $B_c^+ \rightarrow J/\psi$ plus hadrons is also investigated and found negligible. Their individual proportions with respect to the signal yield are determined as

$$\alpha_f = R_f \mathcal{B}_{cascf} R_{\epsilon f}, \quad (6)$$

and then added, $\alpha = \sum_f \alpha_f$, where \mathcal{B}_{cascf} is the sum of the measured branching fractions [40] for the ψ_f state to decay to a J/ψ meson by emission of unreconstructed photons or light hadrons, and $R_{\epsilon f}$ is the ratio of the feeddown and the signal reconstruction efficiencies.³ This quantity is small because of the $m_{J/\psi\mu} > 5.3 \text{ GeV}$ requirement. For χ_{cJ}

³For $B_c^+ \rightarrow J/\psi\tau^+\nu_\tau$, $\mathcal{B}_{cascf} = \mathcal{B}(\tau^+ \rightarrow \mu^+\nu_\mu\bar{\nu}_\tau)$.

Table 1: Values of the parameters affecting the estimate of the feeddown fraction in the fit to the $m_{J/\psi\mu}$ distribution. For $B_c^+ \rightarrow \chi_{cJ}\mu^+\nu_\mu$, $\sum_{J=0,1,2} R_f J \mathcal{B}_{\text{casc}f J}$ is listed.

Feeddown mode	R_f	$\mathcal{B}_{\text{casc}f}$	R_{ef}	α_f
$B_c^+ \rightarrow \psi(2S)\mu^+\nu_\mu$	0.009 – 0.185	0.598 ± 0.006	0.118 ± 0.004	0.0069 ± 0.0062
$B_c^+ \rightarrow \chi_{cJ}\mu^+\nu_\mu$	0.032 – 0.038		0.364 ± 0.009	0.0127 ± 0.0011
$B_c^+ \rightarrow J/\psi\tau^+\nu_\tau$	0.237 – 0.283	0.1741 ± 0.0004	0.014 ± 0.001	0.0006 ± 0.0001
Total α				0.0202 ± 0.0063

states the sum extends over the three J values, $R_f \mathcal{B}_{\text{casc}f} = \sum_{J=0,1,2} R_f J \mathcal{B}_{\text{casc}f J}$. The values of the parameters affecting the estimate of the feeddown fraction are summarized in Table 1. Theoretical predictions for R_f for the $B_c^+ \rightarrow \psi(2S)\mu^+\nu_\mu$ feeddown mode vary over a wide range, 0.009–0.185 [17, 20–22, 24, 41, 42]. An average of the highest and the lowest prediction is taken for the nominal estimate, and half of the difference is taken for the systematic error. The theoretical uncertainties in the $R_f \mathcal{B}_{\text{casc}f}$ values for the dominant $B_c^+ \rightarrow \chi_{cJ}\mu^+\nu_\mu$ feeddown mode are smaller, 0.032–0.038 [23, 43, 44]. The spread is also limited for theoretical predictions of R_f for the $B_c^+ \rightarrow J/\psi\tau^+\nu_\tau$ decay, 0.237–0.283 [18, 21, 23, 44]. The simulated distributions for the individual feeddown modes are mixed according to the proportions resulting from the $R_f \mathcal{B}_{\text{casc}f}$ values and then parameterized as

$$\mathcal{P}_{\text{fd}}(m_{J/\psi\mu}) \propto \text{PS}(m_{J/\psi\mu}) (1 + f_1 \bar{m}_{J/\psi\mu} + f_2 \bar{m}_{J/\psi\mu}^2), \quad (7)$$

where f_1 and f_2 are parameters determined by the fit. The effect of the unreconstructed decay products X is to lower the effective M_{B_c} value in Eq. (5). Varying the feeddown fraction within its uncertainty changes the signal yield by up to 0.6%.

The combinatorial $B_{u,d,s}$ background is parameterized with an exponential function. The tail of the $B_u^+ \rightarrow J/\psi h^+$ distribution, with the light hadron misidentified as a muon, may enter the signal region because of detector resolution. We parameterize it with a Gaussian function, $G(m_{J/\psi\mu})$, with a mean value and width fixed to the results of the fit to the simulated $B_u^+ \rightarrow J/\psi h^+$ distribution. The exponential and $G(m_{J/\psi\mu})$ functions together define $\mathcal{P}_{\text{bkg}}(m_{J/\psi\mu})$,

$$\mathcal{P}_{\text{bkg}}(m_{J/\psi\mu}) \propto c N_e e^{b_1 \bar{m}_{J/\psi\mu} + b_2 \bar{m}_{J/\psi\mu}^2} + (1 - c) G(m_{J/\psi\mu}),$$

where N_e normalizes the exponential function to one. The combinatorial background fraction c and the polynomial coefficients b_1 and b_2 are free parameters in the simultaneous fit to the simulated $B_{u,d,s} \rightarrow J/\psi X$ distribution and to the distribution in the data. To avoid relying on simulation for the absolute values of the muon misidentification rates, c is allowed to vary independently in the fit to the simulated and the observed distributions. A systematic uncertainty of 1.8% is assigned to this background parameterization based on fit results in which either the Gaussian term is neglected or the exponential function is replaced by a sum of two exponential functions.

Varying the upper limit of the mass range used in the fit from 8.0 down to 6.75 GeV, results in a signal yield change of up to 1.5%. Varying the corresponding lower limit from its default value of 5.3 to 5.1 GeV, thus including the peak of the $B_u^+ \rightarrow J/\psi h^+$ component (see Fig. 2), or to 5.5 GeV, thus avoiding the tail of that component, results in a relative change in the \mathcal{R} value of up to 1.6%.

The default method of the $B_c^+ \rightarrow J/\psi \mu^+ \nu_\mu$ signal-yield determination relies on simulation to predict the signal and background shapes in the $m_{J/\psi \mu}$ distribution. An alternative approach relies on simulation to predict the signal and background shapes of the $\Delta_{\text{sig/bkg}}(-2\ln\mathcal{L})$ distribution. Correlations between $m_{J/\psi \mu}$ and $\Delta_{\text{sig/bkg}}(-2\ln\mathcal{L})$ variables are small. The requirement on the $\Delta_{\text{sig/bkg}}(-2\ln\mathcal{L})$ value is removed. The $m_{J/\psi \mu}$ range is restricted to 5.3–6.1 GeV to exclude the backgrounds above the B_c^+ kinematic limit. The signal and combinatorial background yields are determined by a fit to the $\Delta_{\text{sig/bkg}}(-2\ln\mathcal{L})$ distribution in the data. The B_c^+ feeddown simulation predicts a similar $\Delta_{\text{sig/bkg}}(-2\ln\mathcal{L})$ shape as for the $B_c^+ \rightarrow J/\psi \mu^+ \nu_\mu$ signal. Therefore, this contribution is not represented explicitly in the fit to the $\Delta_{\text{sig/bkg}}(-2\ln\mathcal{L})$ distribution, but is subtracted from the fitted signal yield according to the feeddown fraction α . Taking into account the differences in signal efficiency, the $B_c^+ \rightarrow J/\psi \mu^+ \nu_\mu$ signal yield is consistent with that resulting from the $m_{J/\psi \mu}$ fit method within 0.5%, which is included as an additional systematic uncertainty due to the $\Delta_{\text{sig/bkg}}(-2\ln\mathcal{L})$ requirement in the nominal approach.

7 Results

The ratio of the reconstruction efficiencies between the two B_c^+ signal modes, as determined from simulation, is $\epsilon(B_c^+ \rightarrow J/\psi \mu^+ \nu_\mu)/\epsilon(B_c^+ \rightarrow J/\psi \pi^+) = 1.14 \pm 0.01$ (statistical error) for $B_c^+ \rightarrow J/\psi \mu^+ \nu_\mu$ events generated in the endpoint region. Using different $B_c^+ \rightarrow J/\psi \mu^+ \nu_\mu$ form factor models changes this efficiency ratio by up to 1.3%. Efficiencies of the pion and muon particle identification (PID) requirements have systematic uncertainties of 0.8% and 1.9%, respectively. The efficiency-ratio systematic uncertainties from the B_c^+ lifetime assumed in the simulation is 0.2% due to the cancelations between the two decay modes. The fraction of multiple signal candidates per event is 0.1% for $B_c^+ \rightarrow J/\psi \pi^+$ and 1.9% for $B_c^+ \rightarrow J/\psi \mu^+ \nu_\mu$ decays. To check for possible biases due to the neglected correlations between multiple candidates, one candidate is randomly chosen, which changes the \mathcal{R} result by 0.4%. The systematic uncertainty associated with the limited knowledge of the efficiency of the $\Delta_{\text{sig/bkg}}(-2\ln\mathcal{L})$ requirement for $B_c^+ \rightarrow J/\psi \mu^+ \nu_\mu$ decays is included using the results of the $\Delta_{\text{sig/bkg}}(-2\ln\mathcal{L})$ fit. To study the corresponding uncertainty for $B_c^+ \rightarrow J/\psi \pi^+$ decays, the $\Delta_{\text{sig/bkg}}(-2\ln\mathcal{L})$ requirement is varied, resulting in a 2% variation. The systematic uncertainty associated with the trigger simulation is 3.4%, as estimated by modifying the trigger requirements. The systematic errors are summarized in Table 2. The total relative systematic uncertainty on $\mathcal{R}(m_{J/\psi \mu} > 5.3 \text{ GeV})$ is 6%.

The result for the ratio of the branching fractions restricted to decays with $m_{J/\psi \mu} > 5.3 \text{ GeV}$ is

$$\mathcal{R}(m_{J/\psi \mu} > 5.3 \text{ GeV}) = 0.271 \pm 0.016 \pm 0.016, \quad (8)$$

Table 2: Summary of systematic uncertainties. The total systematic errors are obtained by adding in quadrature the individual contributions.

Contribution	Relative error
$m_{J/\psi\pi}$ signal shape	2.3%
$m_{J/\psi\pi}$ background shape	0.2%
$B_c^+ \rightarrow J/\psi K^+$ component	0.1%
$m_{J/\psi\mu}$ signal shape	0.7%
$m_{J/\psi\mu}$ background shape	1.8%
B_c^+ feeddown	0.6%
Lower $m_{J/\psi\mu}$ fit range limit	1.6%
Upper $m_{J/\psi\mu}$ fit range limit	1.5%
$B_c^+ \rightarrow J/\psi \mu^+ \nu_\mu$ model dependence of efficiency	1.3%
Pion PID	0.8%
Muon PID	1.9%
Lifetime	0.2%
Multiple candidates	0.4%
$\Delta_{\text{sig}/\text{bkg}}(-2\ln\mathcal{L})$ requirement for $B_c^+ \rightarrow J/\psi \pi^+$	2.0%
$\Delta_{\text{sig}/\text{bkg}}(-2\ln\mathcal{L})$ requirement for $B_c^+ \rightarrow J/\psi \mu^+ \nu_\mu$	0.5%
Trigger simulation	3.4%
Total within selected $m_{J/\psi\mu}$ range	6.0%
$m_{J/\psi\mu}$ extrapolation	7.9%
Total	9.9%

where the first uncertainty is statistical and the second is systematic. This ratio is extrapolated to the full phase-space as follows. The model of Kiselev *et al.* [21] predicts the fraction of the $B_c^+ \rightarrow J/\psi \mu^+ \nu_\mu$ rate with $m_{J/\psi\mu}$ above 5.3 GeV to be 0.173, which is close to an average over six different models [22, 24, 41, 45, 46]. The largest deviation from this prediction is 7.9%, which is taken as an estimate of the extrapolation systematic error. This increases the systematic uncertainty on \mathcal{R} , when extrapolated to the full mass range, to 9.9% yielding

$$\mathcal{R} = 0.0469 \pm 0.0028 \pm 0.0046. \quad (9)$$

A comparison between the measured and the predicted values of \mathcal{R} is shown in Fig. 4. The measured value is slightly below the lowest predicted value. The predictions by the relativistic quasipotential Schrödinger model of Ebert *et al.* [22] and the model of El-Hady *et al.*, based on a nonrelativistic reduction of the Bethe-Salpeter equation [19], are in good agreement with the experimental value. The model of Ke *et al.* [24], based on the modified harmonic oscillator wave function in light-front quark model, is also consistent with the data. The other models [17, 18, 20, 21, 23] significantly overestimate \mathcal{R} .

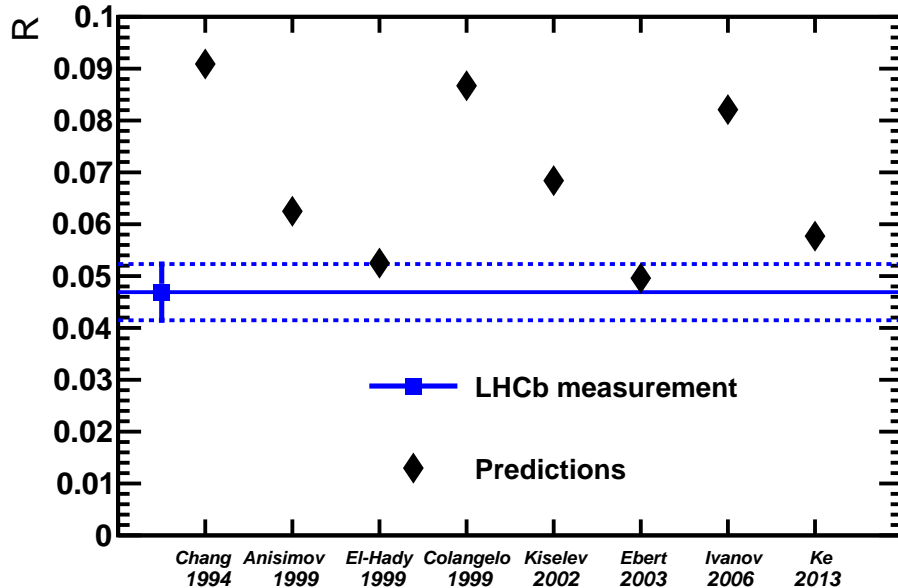


Figure 4: The measured value of \mathcal{R} (horizontal solid line) and its $\pm 1\sigma$ uncertainty band (dashed lines) compared to the predictions (diamonds). A nonrelativistic reduction of the Bethe-Salpeter equation is used in the predictions of Chang *et al.* [17], El-Hady *et al.* [19], and Colangelo *et al.* [20], while the latter also utilizes heavy quark symmetry. A light-front constituent quark model is used by Anisimov *et al.* [18] and Ke *et al.* [24]. QCD sum rules are used by Kiselev *et al.* [21], a relativistic quasipotential Schrödinger model is used by Ebert *et al.* [22], and a relativistic constituent quark model is used by Ivanov *et al.* [23].

8 Summary

The ratio of hadronic and semileptonic decay branching fractions of the B_c^+ meson is measured for the first time. Within the observed mass range, $m_{J/\psi\mu} > 5.3$ GeV, the measured value of $\mathcal{B}(B_c^+ \rightarrow J/\psi\pi^+)/\mathcal{B}(B_c^+ \rightarrow J/\psi\mu^+\nu_\mu)$ is found to be 0.271 ± 0.016 (stat) ± 0.016 (syst). Extrapolating to the full mass range, we obtain a value of $\mathcal{B}(B_c^+ \rightarrow J/\psi\pi^+)/\mathcal{B}(B_c^+ \rightarrow J/\psi\mu^+\nu_\mu) = 0.0469 \pm 0.0028$ (stat) ± 0.0046 (syst), which is in good agreement with the theoretical predictions by Ebert *et al.* [22] and El-Hady *et al.* [19], and consistent with the prediction by Ke *et al.* [24]. All other currently available models [17, 18, 20, 21, 23] overestimate this ratio.

Acknowledgements

We express our gratitude to our colleagues in the CERN accelerator departments for the excellent performance of the LHC. We thank the technical and administrative staff at the LHCb institutes. We acknowledge support from CERN and from the national agencies:

CAPES, CNPq, FAPERJ and FINEP (Brazil); NSFC (China); CNRS/IN2P3 (France); BMBF, DFG, HGF and MPG (Germany); SFI (Ireland); INFN (Italy); FOM and NWO (The Netherlands); MNiSW and NCN (Poland); MEN/IFA (Romania); MinES and FANO (Russia); MinECo (Spain); SNSF and SER (Switzerland); NASU (Ukraine); STFC (United Kingdom); NSF (USA). The Tier1 computing centres are supported by IN2P3 (France), KIT and BMBF (Germany), INFN (Italy), NWO and SURF (The Netherlands), PIC (Spain), GridPP (United Kingdom). We are indebted to the communities behind the multiple open source software packages on which we depend. We are also thankful for the computing resources and the access to software R&D tools provided by Yandex LLC (Russia). Individual groups or members have received support from EPLANET, Marie Skłodowska-Curie Actions and ERC (European Union), Conseil général de Haute-Savoie, Labex ENIGMASS and OCEVU, Région Auvergne (France), RFBR (Russia), XuntaGal and GENCAT (Spain), Royal Society and Royal Commission for the Exhibition of 1851 (United Kingdom).

References

- [1] I. P. Gouz *et al.*, *Prospects for the B_c studies at LHCb*, Phys. Atom. Nucl. **67** (2004) 1559, [arXiv:hep-ph/0211432](#).
- [2] LHCb collaboration, R. Aaij *et al.*, *Observation of the decay $B_c^+ \rightarrow B_s^0 \pi^+$* , Phys. Rev. Lett. **111** (2013) 181801, [arXiv:1308.4544](#).
- [3] CDF collaboration, F. Abe *et al.*, *Observation of the B_c meson in $p\bar{p}$ collisions at $\sqrt{s} = 1.8$ TeV*, Phys. Rev. Lett. **81** (1998) 2432, [arXiv:hep-ex/9805034](#).
- [4] CDF collaboration, A. Abulencia *et al.*, *Measurement of the B_c^+ meson lifetime using the decay mode $B_c^+ \rightarrow J/\psi e^+ \nu_e$* , Phys. Rev. Lett. **97** (2006) 012002, [arXiv:hep-ex/0603027](#).
- [5] D0 collaboration, V. M. Abazov *et al.*, *Measurement of the lifetime of the B_c^\pm meson in the semileptonic decay channel*, Phys. Rev. Lett. **102** (2009) 092001, [arXiv:0805.2614](#).
- [6] LHCb collaboration, R. Aaij *et al.*, *Measurement of the B_c^+ meson lifetime using $B_c^+ \rightarrow J/\psi \mu^+ \nu_\mu X$ decays*, Eur. Phys. J. **C74** (2014) 2839, [arXiv:1401.6932](#).
- [7] CDF collaboration, T. Aaltonen *et al.*, *Measurement of the B_c^- meson lifetime in the decay $B_c^- \rightarrow J/\psi \pi^-$* , Phys. Rev. **D87** (2013) 011101, [arXiv:1210.2366](#).
- [8] CDF collaboration, T. Aaltonen *et al.*, *Observation of the decay $B_c^\pm \rightarrow J/\psi \pi^\pm$ and measurement of the B_c^\pm mass*, Phys. Rev. Lett. **100** (2008) 182002, [arXiv:0712.1506](#).
- [9] D0 collaboration, V. M. Abazov *et al.*, *Observation of the B_c meson in the exclusive decay $B_c \rightarrow J/\psi \pi$* , Phys. Rev. Lett. **101** (2008) 012001, [arXiv:0802.4258](#).

- [10] LHCb collaboration, R. Aaij *et al.*, *Measurements of B_c^+ production and mass with the $B_c^+ \rightarrow J/\psi\pi^+$ decay*, Phys. Rev. Lett. **109** (2012) 232001, arXiv:1209.5634.
- [11] LHCb collaboration, R. Aaij *et al.*, *First observation of the decay $B_c^+ \rightarrow J/\psi\pi^+\pi^-\pi^+$* , Phys. Rev. Lett. **108** (2012) 251802, arXiv:1204.0079.
- [12] LHCb collaboration, R. Aaij *et al.*, *Observation of the decay $B_c^+ \rightarrow \psi(2S)\pi^+$* , Phys. Rev. **D87** (2013) 071103(R), arXiv:1303.1737.
- [13] LHCb collaboration, R. Aaij *et al.*, *Observation of $B_c^+ \rightarrow J/\psi D_s^+$ and $B_c^+ \rightarrow J/\psi D_s^{*+}$ decays*, Phys. Rev. **D87** (2013) 112012, arXiv:1304.4530.
- [14] LHCb collaboration, R. Aaij *et al.*, *First observation of the decay $B_c^+ \rightarrow J/\psi K^+$* , JHEP **09** (2013) 075, arXiv:1306.6723.
- [15] LHCb collaboration, R. Aaij *et al.*, *Observation of the decay $B_c^+ \rightarrow J/\psi K^+ K^- \pi^+$* , JHEP **11** (2013) 094, arXiv:1309.0587.
- [16] LHCb collaboration, R. Aaij *et al.*, *Evidence for the decay $B_c^+ \rightarrow J/\psi 3\pi^+ 2\pi^-$* , JHEP **05** (2014) 148, arXiv:1404.0287.
- [17] C.-H. Chang and Y.-Q. Chen, *Decays of the B_c meson*, Phys. Rev. **D49** (1994) 3399.
- [18] A. Y. Anisimov, I. M. Narodetskii, C. Semay, and B. Silvestre-Blac, *The B_c meson lifetime in the light-front constituent quark model*, Phys. Lett. **B452** (1999) 129, arXiv:hep-ph/9812514; A. Y. Anisimov, P. Y. Kulikov, I. M. Narodetskii, and K. A. Ter-Martirosyan, *Exclusive and inclusive decays of the B_c meson in the light-front ISGW model*, Phys. Atom. Nucl. **62** (1999) 1739, arXiv:hep-ph/9809249.
- [19] A. A. El-Hady, J. H. Muñoz, and J. P. Vary, *Semileptonic and nonleptonic B_c decays*, Phys. Rev. **D62** (1999) 014019, arXiv:hep-ph/9909406.
- [20] P. Colangelo and F. De Fazio, *Using heavy quark spin symmetry in semileptonic B_c decays*, Phys. Rev. **D61** (1999) 034012, arXiv:hep-ph/9909423.
- [21] V. V. Kiselev, *Exclusive decays and lifetime of B_c meson in QCD sum rules*, arXiv:hep-ph/0211021.
- [22] D. Ebert, R. N. Faustov, and V. O. Galkin, *Weak decays of the B_c meson to charmonium and D mesons in the relativistic quark model*, Phys. Rev. **D68** (2003) 094020, arXiv:hep-ph/0306306.
- [23] M. A. Ivanov, J. G. Körner, and P. Santorelli, *Exclusive semileptonic and nonleptonic decays of the B_c meson*, Phys. Rev. **D73** (2006) 054024, arXiv:hep-ph/0602050.
- [24] H.-W. Ke, T. Liu, and X.-Q. Li, *Transitions of $B_c \rightarrow \psi(1S, 2S)$ and the modified harmonic oscillator wave function in LFQM*, Phys. Rev. **D89** (2014) 017501, arXiv:1307.5925.

- [25] LHCb collaboration, A. A. Alves Jr. *et al.*, *The LHCb detector at the LHC*, JINST **3** (2008) S08005.
- [26] R. Aaij *et al.*, *Performance of the LHCb Vertex Locator*, arXiv:1405.7808, submitted to JINST.
- [27] R. Arink *et al.*, *Performance of the LHCb Outer Tracker*, JINST **9** (2014) P01002, arXiv:1311.3893.
- [28] M. Adinolfi *et al.*, *Performance of the LHCb RICH detector at the LHC*, Eur. Phys. J. **C73** (2013) 2431, arXiv:1211.6759.
- [29] A. A. Alves Jr. *et al.*, *Performance of the LHCb muon system*, JINST **8** (2013) P02022, arXiv:1211.1346.
- [30] T. Sjöstrand, S. Mrenna, and P. Skands, *PYTHIA 6.4 physics and manual*, JHEP **05** (2006) 026, arXiv:hep-ph/0603175.
- [31] I. Belyaev *et al.*, *Handling of the generation of primary events in GAUSS, the LHCb simulation framework*, Nuclear Science Symposium Conference Record (NSS/MIC) **IEEE** (2010) 1155.
- [32] C.-H. Chang, C. Driouichi, P. Eerola, and X. G. Wu, *BCVEGPY: an event generator for hadronic production of the B_c^+ meson*, Comput. Phys. Commun. **159** (2004) 192, arXiv:hep-ph/0309120.
- [33] D. J. Lange, *The EvtGen particle decay simulation package*, Nucl. Instrum. Meth. **A462** (2001) 152.
- [34] P. Golonka and Z. Was, *PHOTOS Monte Carlo: a precision tool for QED corrections in Z and W decays*, Eur. Phys. J. **C45** (2006) 97, arXiv:hep-ph/0506026.
- [35] GEANT4 collaboration, J. Allison *et al.*, *Geant4 developments and applications*, IEEE Trans. Nucl. Sci. **53** (2006) 270; GEANT4 collaboration, S. Agostinelli *et al.*, *GEANT4: A simulation toolkit*, Nucl. Instrum. Meth. **A506** (2003) 250.
- [36] M. Clemencic *et al.*, *The LHCb simulation application, GAUSS: design, evolution and experience*, J. of Phys. : Conf. Ser. **331** (2011) 032023.
- [37] R. Aaij *et al.*, *The LHCb trigger and its performance in 2011*, JINST **8** (2013) P04022, arXiv:1211.3055.
- [38] M. Adinolfi *et al.*, *Performance of the LHCb RICH detector at the LHC*, arXiv:1211.6759.
- [39] T. Skwarnicki, *A study of the radiative cascade transitions between the Upsilon-prime and Upsilon resonances*, PhD thesis, Institute of Nuclear Physics, Krakow, 1986, DESY-F31-86-02.

- [40] Particle Data Group, J. Beringer *et al.*, *Review of particle physics*, Phys. Rev. **D86** (2012) 010001, and 2013 partial update for the 2014 edition.
- [41] D. Scora and N. Isgur, *Semileptonic meson decays in the quark model: an update*, Phys. Rev. **D52** (1995) 2783, [arXiv:hep-ph/9503486](#).
- [42] J.-F. Liu and K.-T. Chao, *B_c meson weak decays and CP violation*, Phys. Rev. **D56** (1997) 4133.
- [43] C.-H. Chang, Y.-Q. Chen, G.-L. Wang, and H.-S. Zong, *Decays of the meson B_c to a P – wave charmonium state χ_c or h_c* , Phys. Rev. **D65** (2001) 014017, [arXiv:hep-ph/0103036](#).
- [44] E. Hernandez, J. Nieves, and J. M. Verde-Velasco, *Study of exclusive semileptonic and nonleptonic decays of B_c^- in a nonrelativistic quark model*, Phys. Rev. **D74** (2006) 074008, [arXiv:hep-ph/0607150](#).
- [45] W. Wang, Y.-L. Shen, and C.-D. Lü, *Covariant light-front approach for B_c transition form factors*, Phys. Rev. **D79** (2009) 054012, [arXiv:0811.3748](#).
- [46] W.-F. Wang, Y.-Y. Fan, and Z.-J. Xiao, *Semileptonic decays $B_c \rightarrow (\eta_c, J/\psi)\ell\nu$ in the perturbative QCD approach*, [arXiv:1212.5903](#).

LHCb collaboration

R. Aaij⁴¹, B. Adeva³⁷, M. Adinolfi⁴⁶, A. Affolder⁵², Z. Ajaltouni⁵, S. Akar⁶, J. Albrecht⁹, F. Alessio³⁸, M. Alexander⁵¹, S. Ali⁴¹, G. Alkhazov³⁰, P. Alvarez Cartelle³⁷, A.A. Alves Jr^{25,38}, S. Amato², S. Amerio²², Y. Amhis⁷, L. An³, L. Anderlini^{17,g}, J. Anderson⁴⁰, R. Andreassen⁵⁷, M. Andreotti^{16,f}, J.E. Andrews⁵⁸, R.B. Appleby⁵⁴, O. Aquines Gutierrez¹⁰, F. Archilli³⁸, A. Artamonov³⁵, M. Artuso⁵⁹, E. Aslanides⁶, G. Auriemma^{25,n}, M. Baalouch⁵, S. Bachmann¹¹, J.J. Back⁴⁸, A. Badalov³⁶, V. Balagura³¹, W. Baldini¹⁶, R.J. Barlow⁵⁴, C. Barschel³⁸, S. Barsuk⁷, W. Barter⁴⁷, V. Batozskaya²⁸, V. Battista³⁹, A. Bay³⁹, L. Beaucourt⁴, J. Beddow⁵¹, F. Bedeschi²³, I. Bediaga¹, S. Belogurov³¹, K. Belous³⁵, I. Belyaev³¹, E. Ben-Haim⁸, G. Bencivenni¹⁸, S. Benson³⁸, J. Benton⁴⁶, A. Berezhnoy³², R. Bernet⁴⁰, M.-O. Bettler⁴⁷, M. van Beuzekom⁴¹, A. Bien¹¹, S. Bifani⁴⁵, T. Bird⁵⁴, A. Bizzeti^{17,i}, P.M. Bjørnstad⁵⁴, T. Blake⁴⁸, F. Blanc³⁹, J. Blouw¹⁰, S. Blusk⁵⁹, V. Bocci²⁵, A. Bondar³⁴, N. Bondar^{30,38}, W. Bonivento^{15,38}, S. Borghi⁵⁴, A. Borgia⁵⁹, M. Borsato⁷, T.J.V. Bowcock⁵², E. Bowen⁴⁰, C. Bozzi¹⁶, T. Brambach⁹, J. van den Brand⁴², J. Bressieux³⁹, D. Brett⁵⁴, M. Britsch¹⁰, T. Britton⁵⁹, J. Brodzicka⁵⁴, N.H. Brook⁴⁶, H. Brown⁵², A. Bursche⁴⁰, G. Busetto^{22,r}, J. Buytaert³⁸, S. Cadeddu¹⁵, R. Calabrese^{16,f}, M. Calvi^{20,k}, M. Calvo Gomez^{36,p}, P. Campana^{18,38}, D. Campora Perez³⁸, A. Carbone^{14,d}, G. Carboni^{24,l}, R. Cardinale^{19,38,j}, A. Cardini¹⁵, L. Carson⁵⁰, K. Carvalho Akiba², G. Casse⁵², L. Cassina²⁰, L. Castillo Garcia³⁸, M. Cattaneo³⁸, Ch. Cauet⁹, R. Cenci⁵⁸, M. Charles⁸, Ph. Charpentier³⁸, S. Chen⁵⁴, S.-F. Cheung⁵⁵, N. Chiapolini⁴⁰, M. Chrzaszcz^{40,26}, K. Ciba³⁸, X. Cid Vidal³⁸, G. Ciezarek⁵³, P.E.L. Clarke⁵⁰, M. Clemencic³⁸, H.V. Cliff⁴⁷, J. Closier³⁸, V. Coco³⁸, J. Cogan⁶, E. Cogneras⁵, P. Collins³⁸, A. Comerma-Montells¹¹, A. Contu¹⁵, A. Cook⁴⁶, M. Coombes⁴⁶, S. Coquereau⁸, G. Corti³⁸, M. Corvo^{16,f}, I. Counts⁵⁶, B. Couturier³⁸, G.A. Cowan⁵⁰, D.C. Craik⁴⁸, M. Cruz Torres⁶⁰, S. Cunliffe⁵³, R. Currie⁵⁰, C. D'Ambrosio³⁸, J. Dalseno⁴⁶, P. David⁸, P.N.Y. David⁴¹, A. Davis⁵⁷, K. De Bruyn⁴¹, S. De Capua⁵⁴, M. De Cian¹¹, J.M. De Miranda¹, L. De Paula², W. De Silva⁵⁷, P. De Simone¹⁸, D. Decamp⁴, M. Deckenhoff⁹, L. Del Buono⁸, N. Déléage⁴, D. Derkach⁵⁵, O. Deschamps⁵, F. Dettori³⁸, A. Di Canto³⁸, H. Dijkstra³⁸, S. Donleavy⁵², F. Dordei¹¹, M. Dorigo³⁹, A. Dosil Suárez³⁷, D. Dossett⁴⁸, A. Dovbnya⁴³, K. Dreimanis⁵², G. Dujany⁵⁴, F. Dupertuis³⁹, P. Durante³⁸, R. Dzhelyadin³⁵, A. Dziurda²⁶, A. Dzyuba³⁰, S. Easo^{49,38}, U. Egede⁵³, V. Egorychev³¹, S. Eidelman³⁴, S. Eisenhardt⁵⁰, U. Eitschberger⁹, R. Ekelhof⁹, L. Eklund^{51,38}, I. El Rifai⁵, Ch. Elsasser⁴⁰, S. Ely⁵⁹, S. Esen¹¹, H.-M. Evans⁴⁷, T. Evans⁵⁵, A. Falabella¹⁴, C. Färber¹¹, C. Farinelli⁴¹, N. Farley⁴⁵, S. Farry⁵², R.F. Fay⁵², D. Ferguson⁵⁰, V. Fernandez Albor³⁷, F. Ferreira Rodrigues¹, M. Ferro-Luzzi³⁸, S. Filippov³³, M. Fiore^{16,f}, M. Fiorini^{16,f}, M. Firlej²⁷, C. Fitzpatrick³⁸, T. Fiutowski²⁷, M. Fontana¹⁰, F. Fontanelli^{19,j}, R. Forty³⁸, O. Francisco², M. Frank³⁸, C. Frei³⁸, M. Frosini^{17,38,g}, J. Fu^{21,38}, E. Furfaro^{24,l}, A. Gallas Torreira³⁷, D. Galli^{14,d}, S. Gallorini²², S. Gambetta^{19,j}, M. Gandelman², P. Gandini⁵⁹, Y. Gao³, J. García Pardiñas³⁷, J. Garofoli⁵⁹, J. Garra Tico⁴⁷, L. Garrido³⁶, C. Gaspar³⁸, R. Gauld⁵⁵, L. Gavardi⁹, G. Gavrillov³⁰, E. Gersabeck¹¹, M. Gersabeck⁵⁴, T. Gershon⁴⁸, Ph. Ghez⁴, A. Gianelle²², S. Giani³⁹, V. Gibson⁴⁷, L. Giubega²⁹, V.V. Gligorov³⁸, C. Göbel⁶⁰, D. Golubkov³¹, A. Golutvin^{53,31,38}, A. Gomes^{1,a}, H. Gordon³⁸, C. Gotti²⁰, M. Grabalosa Gándara⁵, R. Graciani Diaz³⁶, L.A. Granado Cardoso³⁸, E. Graugés³⁶, G. Graziani¹⁷, A. Grecu²⁹, E. Greening⁵⁵, S. Gregson⁴⁷, P. Griffith⁴⁵, L. Grillo¹¹, O. Grünberg⁶², B. Gui⁵⁹, E. Gushchin³³, Yu. Guz^{35,38}, T. Gys³⁸, C. Hadjivasiliou⁵⁹, G. Haefeli³⁹, C. Haen³⁸, S.C. Haines⁴⁷, S. Hall⁵³, B. Hamilton⁵⁸, T. Hampson⁴⁶, X. Han¹¹, S. Hansmann-Menzemer¹¹, N. Harnew⁵⁵, S.T. Harnew⁴⁶, J. Harrison⁵⁴,

J. He³⁸, T. Head³⁸, V. Heijne⁴¹, K. Hennessy⁵², P. Henrard⁵, L. Henry⁸,
 J.A. Hernando Morata³⁷, E. van Herwijnen³⁸, M. Heß⁶², A. Hicheur¹, D. Hill⁵⁵, M. Hoballah⁵,
 C. Hombach⁵⁴, W. Hulsbergen⁴¹, P. Hunt⁵⁵, N. Hussain⁵⁵, D. Hutchcroft⁵², D. Hynds⁵¹,
 M. Idzik²⁷, P. Ilten⁵⁶, R. Jacobsson³⁸, A. Jaeger¹¹, J. Jalocha⁵⁵, E. Jans⁴¹, P. Jatón³⁹,
 A. Jawahery⁵⁸, F. Jing³, M. John⁵⁵, D. Johnson⁵⁵, C.R. Jones⁴⁷, C. Joram³⁸, B. Jost³⁸,
 N. Jurik⁵⁹, M. Kabbalo⁹, S. Kandybei⁴³, W. Kanso⁶, M. Karacson³⁸, T.M. Karbach³⁸,
 S. Karodia⁵¹, M. Kelsey⁵⁹, I.R. Kenyon⁴⁵, T. Ketel⁴², B. Khanji²⁰, C. Khurewathanakul³⁹,
 S. Klaver⁵⁴, K. Klimaszewski²⁸, O. Kochebina⁷, M. Kolpin¹¹, I. Komarov³⁹, R.F. Koopman⁴²,
 P. Koppenburg^{41,38}, M. Korolev³², A. Kozlinskiy⁴¹, L. Kravchuk³³, K. Kreplin¹¹, M. Krepis⁴⁸,
 G. Krocker¹¹, P. Krokovny³⁴, F. Kruse⁹, W. Kucewicz^{26,o}, M. Kucharczyk^{20,26,38,k},
 V. Kudryavtsev³⁴, K. Kurek²⁸, T. Kvaratskheliya³¹, V.N. La Thi³⁹, D. Lacarrere³⁸, G. Lafferty⁵⁴,
 A. Lai¹⁵, D. Lambert⁵⁰, R.W. Lambert⁴², G. Lanfranchi¹⁸, C. Langenbruch⁴⁸, B. Langhans³⁸,
 T. Latham⁴⁸, C. Lazzeroni⁴⁵, R. Le Gac⁶, J. van Leerdam⁴¹, J.-P. Lees⁴, R. Lefèvre⁵,
 A. Leflat³², J. Lefrançois⁷, S. Leo²³, O. Leroy⁶, T. Lesiak²⁶, B. Leverington¹¹, Y. Li³,
 T. Likhomanenko⁶³, M. Liles⁵², R. Lindner³⁸, C. Linn³⁸, F. Lionetto⁴⁰, B. Liu¹⁵, G. Liu³⁸,
 S. Lohn³⁸, I. Longstaff⁵¹, J.H. Lopes², N. Lopez-March³⁹, P. Lowdon⁴⁰, H. Lu³, D. Lucchesi^{22,r},
 H. Luo⁵⁰, A. Lupato²², E. Luppi^{16,f}, O. Lupton⁵⁵, F. Machefert⁷, I.V. Machikhiliyan³¹,
 F. Maciuc²⁹, O. Maev³⁰, S. Malde⁵⁵, G. Manca^{15,e}, G. Mancinelli⁶, J. Maratas⁵, J.F. Marchand⁴,
 U. Marconi¹⁴, C. Marin Benito³⁶, P. Marino^{23,t}, R. Märki³⁹, J. Marks¹¹, G. Martellotti²⁵,
 A. Martens⁸, A. Martín Sánchez⁷, M. Martinelli⁴¹, D. Martinez Santos⁴², F. Martinez Vidal⁶⁴,
 D. Martins Tostes², A. Massafferri¹, R. Matev³⁸, Z. Mathe³⁸, C. Matteuzzi²⁰, A. Mazurov^{16,f},
 M. McCann⁵³, J. McCarthy⁴⁵, A. McNab⁵⁴, R. McNulty¹², B. McSkelly⁵², B. Meadows⁵⁷,
 F. Meier⁹, M. Meissner¹¹, M. Merk⁴¹, D.A. Milanes⁸, M.-N. Minard⁴, N. Moggi¹⁴,
 J. Molina Rodriguez⁶⁰, S. Monteil⁵, M. Morandin²², P. Morawski²⁷, A. Mordà⁶, M.J. Morello^{23,t},
 J. Moron²⁷, A.-B. Morris⁵⁰, R. Mountain⁵⁹, F. Muheim⁵⁰, K. Müller⁴⁰, M. Mussini¹⁴,
 B. Muster³⁹, P. Naik⁴⁶, T. Nakada³⁹, R. Nandakumar⁴⁹, I. Nasteva², M. Needham⁵⁰, N. Neri²¹,
 S. Neubert³⁸, N. Neufeld³⁸, M. Neuner¹¹, A.D. Nguyen³⁹, T.D. Nguyen³⁹, C. Nguyen-Mau^{39,q},
 M. Nicol⁷, V. Niess⁵, R. Niet⁹, N. Nikitin³², T. Nikodem¹¹, A. Novoselov³⁵, D.P. O’Hanlon⁴⁸,
 A. Oblakowska-Mucha²⁷, V. Obraztsov³⁵, S. Oggero⁴¹, S. Ogilvy⁵¹, O. Okhrimenko⁴⁴,
 R. Oldeman^{15,e}, G. Onderwater⁶⁵, M. Orlandea²⁹, J.M. Otalora Goicochea², P. Owen⁵³,
 A. Oyanguren⁶⁴, B.K. Pal⁵⁹, A. Palano^{13,c}, F. Palombo^{21,u}, M. Palutan¹⁸, J. Panman³⁸,
 A. Papanestis^{49,38}, M. Pappagallo⁵¹, C. Parkes⁵⁴, C.J. Parkinson^{9,45}, G. Passaleva¹⁷,
 G.D. Patel⁵², M. Patel⁵³, C. Patrignani^{19,j}, A. Pazos Alvarez³⁷, A. Pearce⁵⁴, A. Pellegrino⁴¹,
 M. Pepe Altarelli³⁸, S. Perazzini^{14,d}, E. Perez Trigo³⁷, P. Perret⁵, M. Perrin-Terrin⁶,
 L. Pescatore⁴⁵, E. Pesen⁶⁶, K. Petridis⁵³, A. Petrolini^{19,j}, E. Picatoste Olloqui³⁶, B. Pietrzyk⁴,
 T. Pilar⁴⁸, D. Pinci²⁵, A. Pistone¹⁹, S. Playfer⁵⁰, M. Plo Casasus³⁷, F. Polci⁸, A. Poluektov^{48,34},
 E. Polcarpo², A. Popov³⁵, D. Popov¹⁰, B. Popovici²⁹, C. Potterat², E. Price⁴⁶,
 J. Prisciandaro³⁹, A. Pritchard⁵², C. Prouve⁴⁶, V. Pugatch⁴⁴, A. Puig Navarro³⁹, G. Punzi^{23,s},
 W. Qian⁴, B. Rachwal²⁶, J.H. Rademacker⁴⁶, B. Rakotomiamanana³⁹, M. Rama¹⁸,
 M.S. Rangel², I. Raniuk⁴³, N. Rauschmayr³⁸, G. Raven⁴², S. Reichert⁵⁴, M.M. Reid⁴⁸,
 A.C. dos Reis¹, S. Ricciardi⁴⁹, S. Richards⁴⁶, M. Rihl³⁸, K. Rinnert⁵², V. Rives Molina³⁶,
 D.A. Roa Romero⁵, P. Robbe⁷, A.B. Rodrigues¹, E. Rodrigues⁵⁴, P. Rodriguez Perez⁵⁴,
 S. Roiser³⁸, V. Romanovsky³⁵, A. Romero Vidal³⁷, M. Rotondo²², J. Rouvinet³⁹, T. Ruf³⁸,
 F. Ruffini²³, H. Ruiz³⁶, P. Ruiz Valls⁶⁴, J.J. Saborido Silva³⁷, N. Sagidova³⁰, P. Sail⁵¹,
 B. Saitta^{15,e}, V. Salustino Guimaraes², C. Sanchez Mayordomo⁶⁴, B. Sanmartin Sedes³⁷,
 R. Santacesaria²⁵, C. Santamarina Rios³⁷, E. Santovetti^{24,l}, A. Sarti^{18,m}, C. Satriano^{25,n},

A. Satta²⁴, D.M. Saunders⁴⁶, M. Savrie^{16,f}, D. Savrina^{31,32}, M. Schiller⁴², H. Schindler³⁸, M. Schlupp⁹, M. Schmelling¹⁰, B. Schmidt³⁸, O. Schneider³⁹, A. Schopper³⁸, M.-H. Schune⁷, R. Schwemmer³⁸, B. Sciascia¹⁸, A. Sciubba²⁵, M. Seco³⁷, A. Semennikov³¹, I. Sepp⁵³, N. Serra⁴⁰, J. Serrano⁶, L. Sestini²², P. Seyfert¹¹, M. Shapkin³⁵, I. Shapoval^{16,43,f}, Y. Shcheglov³⁰, T. Shears⁵², L. Shekhtman³⁴, V. Shevchenko⁶³, A. Shires⁹, R. Silva Coutinho⁴⁸, G. Simi²², M. Sirendi⁴⁷, N. Skidmore⁴⁶, T. Skwarnicki⁵⁹, N.A. Smith⁵², E. Smith^{55,49}, E. Smith⁵³, J. Smith⁴⁷, M. Smith⁵⁴, H. Snoek⁴¹, M.D. Sokoloff⁵⁷, F.J.P. Soler⁵¹, F. Soomro³⁹, D. Souza⁴⁶, B. Souza De Paula², B. Spaan⁹, A. Sparkes⁵⁰, P. Spradlin⁵¹, S. Sridharan³⁸, F. Stagni³⁸, M. Stahl¹¹, S. Stahl¹¹, O. Steinkamp⁴⁰, O. Stenyakin³⁵, S. Stevenson⁵⁵, S. Stoica²⁹, S. Stone⁵⁹, B. Storaci⁴⁰, S. Stracka^{23,38}, M. Straticiu²⁹, U. Straumann⁴⁰, R. Stroili²², V.K. Subbiah³⁸, L. Sun⁵⁷, W. Sutcliffe⁵³, K. Swientek²⁷, S. Swientek⁹, V. Syropoulos⁴², M. Szczekowski²⁸, P. Szczypka^{39,38}, D. Szilard², T. Szumlak²⁷, S. T'Jampens⁴, M. Teklishyn⁷, G. Tellarini^{16,f}, F. Teubert³⁸, C. Thomas⁵⁵, E. Thomas³⁸, J. van Tilburg⁴¹, V. Tisserand⁴, M. Tobin³⁹, S. Tolk⁴², L. Tomassetti^{16,f}, D. Tonelli³⁸, S. Topp-Joergensen⁵⁵, N. Torr⁵⁵, E. Tournefier⁴, S. Tourneur³⁹, M.T. Tran³⁹, M. Tresch⁴⁰, A. Tsaregorodtsev⁶, P. Tsopelas⁴¹, N. Tuning⁴¹, M. Ubeda Garcia³⁸, A. Ukleja²⁸, A. Ustyuzhanin⁶³, U. Uwer¹¹, V. Vagnoni¹⁴, G. Valenti¹⁴, A. Vallier⁷, R. Vazquez Gomez¹⁸, P. Vazquez Regueiro³⁷, C. Vázquez Sierra³⁷, S. Vecchi¹⁶, J.J. Velthuis⁴⁶, M. Veltri^{17,h}, G. Veneziano³⁹, M. Vesterinen¹¹, B. Viaud⁷, D. Vieira², M. Vieites Diaz³⁷, X. Vilasis-Cardona^{36,p}, A. Vollhardt⁴⁰, D. Volyanskyy¹⁰, D. Voong⁴⁶, A. Vorobyev³⁰, V. Vorobyev³⁴, C. Voß⁶², H. Voss¹⁰, J.A. de Vries⁴¹, R. Waldi⁶², C. Wallace⁴⁸, R. Wallace¹², J. Walsh²³, S. Wandernoth¹¹, J. Wang⁵⁹, D.R. Ward⁴⁷, N.K. Watson⁴⁵, D. Websdale⁵³, M. Whitehead⁴⁸, J. Wicht³⁸, D. Wiedner¹¹, G. Wilkinson⁵⁵, M.P. Williams⁴⁵, M. Williams⁵⁶, F.F. Wilson⁴⁹, J. Wimberley⁵⁸, J. Wishahi⁹, W. Wislicki²⁸, M. Witek²⁶, G. Wormser⁷, S.A. Wotton⁴⁷, S. Wright⁴⁷, S. Wu³, K. Wyllie³⁸, Y. Xie⁶¹, Z. Xing⁵⁹, Z. Xu³⁹, Z. Yang³, X. Yuan³, O. Yushchenko³⁵, M. Zangoli¹⁴, M. Zavertyaev^{10,b}, L. Zhang⁵⁹, W.C. Zhang¹², Y. Zhang³, A. Zhelezov¹¹, A. Zhokhov³¹, L. Zhong³, A. Zvyagin³⁸.

¹ Centro Brasileiro de Pesquisas Físicas (CBPF), Rio de Janeiro, Brazil

² Universidade Federal do Rio de Janeiro (UFRJ), Rio de Janeiro, Brazil

³ Center for High Energy Physics, Tsinghua University, Beijing, China

⁴ LAPP, Université de Savoie, CNRS/IN2P3, Annecy-Le-Vieux, France

⁵ Clermont Université, Université Blaise Pascal, CNRS/IN2P3, LPC, Clermont-Ferrand, France

⁶ CPPM, Aix-Marseille Université, CNRS/IN2P3, Marseille, France

⁷ LAL, Université Paris-Sud, CNRS/IN2P3, Orsay, France

⁸ LPNHE, Université Pierre et Marie Curie, Université Paris Diderot, CNRS/IN2P3, Paris, France

⁹ Fakultät Physik, Technische Universität Dortmund, Dortmund, Germany

¹⁰ Max-Planck-Institut für Kernphysik (MPIK), Heidelberg, Germany

¹¹ Physikalisches Institut, Ruprecht-Karls-Universität Heidelberg, Heidelberg, Germany

¹² School of Physics, University College Dublin, Dublin, Ireland

¹³ Sezione INFN di Bari, Bari, Italy

¹⁴ Sezione INFN di Bologna, Bologna, Italy

¹⁵ Sezione INFN di Cagliari, Cagliari, Italy

¹⁶ Sezione INFN di Ferrara, Ferrara, Italy

¹⁷ Sezione INFN di Firenze, Firenze, Italy

¹⁸ Laboratori Nazionali dell'INFN di Frascati, Frascati, Italy

¹⁹ Sezione INFN di Genova, Genova, Italy

²⁰ Sezione INFN di Milano Bicocca, Milano, Italy

²¹ Sezione INFN di Milano, Milano, Italy

²² Sezione INFN di Padova, Padova, Italy

- ²³ *Sezione INFN di Pisa, Pisa, Italy*
- ²⁴ *Sezione INFN di Roma Tor Vergata, Roma, Italy*
- ²⁵ *Sezione INFN di Roma La Sapienza, Roma, Italy*
- ²⁶ *Henryk Niewodniczanski Institute of Nuclear Physics Polish Academy of Sciences, Kraków, Poland*
- ²⁷ *AGH - University of Science and Technology, Faculty of Physics and Applied Computer Science, Kraków, Poland*
- ²⁸ *National Center for Nuclear Research (NCBJ), Warsaw, Poland*
- ²⁹ *Horia Hulubei National Institute of Physics and Nuclear Engineering, Bucharest-Magurele, Romania*
- ³⁰ *Petersburg Nuclear Physics Institute (PNPI), Gatchina, Russia*
- ³¹ *Institute of Theoretical and Experimental Physics (ITEP), Moscow, Russia*
- ³² *Institute of Nuclear Physics, Moscow State University (SINP MSU), Moscow, Russia*
- ³³ *Institute for Nuclear Research of the Russian Academy of Sciences (INR RAN), Moscow, Russia*
- ³⁴ *Budker Institute of Nuclear Physics (SB RAS) and Novosibirsk State University, Novosibirsk, Russia*
- ³⁵ *Institute for High Energy Physics (IHEP), Protvino, Russia*
- ³⁶ *Universitat de Barcelona, Barcelona, Spain*
- ³⁷ *Universidad de Santiago de Compostela, Santiago de Compostela, Spain*
- ³⁸ *European Organization for Nuclear Research (CERN), Geneva, Switzerland*
- ³⁹ *Ecole Polytechnique Fédérale de Lausanne (EPFL), Lausanne, Switzerland*
- ⁴⁰ *Physik-Institut, Universität Zürich, Zürich, Switzerland*
- ⁴¹ *Nikhef National Institute for Subatomic Physics, Amsterdam, The Netherlands*
- ⁴² *Nikhef National Institute for Subatomic Physics and VU University Amsterdam, Amsterdam, The Netherlands*
- ⁴³ *NSC Kharkiv Institute of Physics and Technology (NSC KIPT), Kharkiv, Ukraine*
- ⁴⁴ *Institute for Nuclear Research of the National Academy of Sciences (KINR), Kyiv, Ukraine*
- ⁴⁵ *University of Birmingham, Birmingham, United Kingdom*
- ⁴⁶ *H.H. Wills Physics Laboratory, University of Bristol, Bristol, United Kingdom*
- ⁴⁷ *Cavendish Laboratory, University of Cambridge, Cambridge, United Kingdom*
- ⁴⁸ *Department of Physics, University of Warwick, Coventry, United Kingdom*
- ⁴⁹ *STFC Rutherford Appleton Laboratory, Didcot, United Kingdom*
- ⁵⁰ *School of Physics and Astronomy, University of Edinburgh, Edinburgh, United Kingdom*
- ⁵¹ *School of Physics and Astronomy, University of Glasgow, Glasgow, United Kingdom*
- ⁵² *Oliver Lodge Laboratory, University of Liverpool, Liverpool, United Kingdom*
- ⁵³ *Imperial College London, London, United Kingdom*
- ⁵⁴ *School of Physics and Astronomy, University of Manchester, Manchester, United Kingdom*
- ⁵⁵ *Department of Physics, University of Oxford, Oxford, United Kingdom*
- ⁵⁶ *Massachusetts Institute of Technology, Cambridge, MA, United States*
- ⁵⁷ *University of Cincinnati, Cincinnati, OH, United States*
- ⁵⁸ *University of Maryland, College Park, MD, United States*
- ⁵⁹ *Syracuse University, Syracuse, NY, United States*
- ⁶⁰ *Pontifícia Universidade Católica do Rio de Janeiro (PUC-Rio), Rio de Janeiro, Brazil, associated to ²*
- ⁶¹ *Institute of Particle Physics, Central China Normal University, Wuhan, Hubei, China, associated to ³*
- ⁶² *Institut für Physik, Universität Rostock, Rostock, Germany, associated to ¹¹*
- ⁶³ *National Research Centre Kurchatov Institute, Moscow, Russia, associated to ³¹*
- ⁶⁴ *Instituto de Fisica Corpuscular (IFIC), Universitat de Valencia-CSIC, Valencia, Spain, associated to ³⁶*
- ⁶⁵ *KVI - University of Groningen, Groningen, The Netherlands, associated to ⁴¹*
- ⁶⁶ *Celal Bayar University, Manisa, Turkey, associated to ³⁸*

^a *Universidade Federal do Triângulo Mineiro (UFMT), Uberaba-MG, Brazil*

^b *P.N. Lebedev Physical Institute, Russian Academy of Science (LPI RAS), Moscow, Russia*

^c *Università di Bari, Bari, Italy*

^d *Università di Bologna, Bologna, Italy*

^e *Università di Cagliari, Cagliari, Italy*

- ^f *Università di Ferrara, Ferrara, Italy*
^g *Università di Firenze, Firenze, Italy*
^h *Università di Urbino, Urbino, Italy*
ⁱ *Università di Modena e Reggio Emilia, Modena, Italy*
^j *Università di Genova, Genova, Italy*
^k *Università di Milano Bicocca, Milano, Italy*
^l *Università di Roma Tor Vergata, Roma, Italy*
^m *Università di Roma La Sapienza, Roma, Italy*
ⁿ *Università della Basilicata, Potenza, Italy*
^o *AGH - University of Science and Technology, Faculty of Computer Science, Electronics and Telecommunications, Kraków, Poland*
^p *LIFAELS, La Salle, Universitat Ramon Llull, Barcelona, Spain*
^q *Hanoi University of Science, Hanoi, Viet Nam*
^r *Università di Padova, Padova, Italy*
^s *Università di Pisa, Pisa, Italy*
^t *Scuola Normale Superiore, Pisa, Italy*
^u *Università degli Studi di Milano, Milano, Italy*